Journal of the Physical Society of Japan **81** (2012) 044701 **FULL PAPERS**
DOI: 10.1143/JPSJ.81.044701

Heavy-Electron Formation and Polaron–Bipolaron Transition in the Anharmonic Holstein Model

Takahiro FUSE[1], Yoshiaki ŌNO[2], and Takashi HOTTA[1,3]

[1]*Department of Physics, Tokyo Metropolitan University, Hachioji, Tokyo 192-0397, Japan*
[2]*Department of Physics, Niigata University, Niigata 950-2181, Japan*
[3]*Advanced Science Research Center, Japan Atomic Energy Agency, Tokai, Ibaraki 319-1195, Japan*

(Received October 3, 2011; accepted January 16, 2012; published online March 7, 2012)

The emergence of the bipolaronic phase and the formation of the heavy-electron state in the anharmonic Holstein model are investigated using the dynamical mean-field theory in combination with the exact diagonalization method. For a weak anharmonicity, it is confirmed that the first-order polaron–bipolaron transition occurs from the observation of a discontinuity in the behavior of several physical quantities. When the anharmonicity is gradually increased, the polaron–bipolaron transition temperature is reduced as well as the critical values of the electron–phonon coupling constant for polaron–bipolaron transition. For a strong anharmonicity, the polaron–bipolaron transition eventually changes to a crossover behavior. The effect of anharmonicity on the formation of the heavy-electron state near the polaron–bipolaron transition and the crossover region is discussed in detail.

KEYWORDS: heavy electron, anharmonicity, rattling, bipolaron, dynamical mean-field theory

1. Introduction

Recently, heavy-electron phenomena have attracted renewed attention in the research field of condensed matter physics.[1)] A traditional mechanism of the emergence of the heavy-electron state is based on quantum criticality induced by the competition between the Kondo effect and Ruderman–Kittel–Kasuya–Yosida interaction. The Kondo effect due to local magnetic moment has been well understood,[2)] but the Kondo-like phenomenon occurs in a more general manner, when a localized entity with internal degrees of freedom is embedded in a conduction electron system and quantum-mechanical exchange interaction effectively works between local degrees of freedom and conduction electrons.

In particular, the Kondo phenomenon with a phonon origin has been potentially discussed. First, Kondo himself has considered a conduction electron system coupled with a local double-well potential.[3,4)] Having two possible electron position in a double-well potential play roles in pseudo-spins, and the Kondo-like behavior is considered to appear in such a two-level system. In fact, it has been shown that the two-level Kondo system exhibits the same behavior as the magnetic Kondo effect.[5–7)] Another important issue regarding the Kondo effect with a phonon origin has been shown by Yu and Anderson.[8)] They have pointed out that the scattering process between spinless *s*-wave conduction electrons to *p*-wave ones is induced by ion displacement. The model proposed by Yu and Anderson has been shown to be mapped to the two-level Kondo model at low temperatures.[9,10)]

A recent revival of research on the Kondo effect with a phonon origin has been triggered by active experimental investigations on cage structure compounds such as filled skutterudites,[11–14)] clathrates,[15–20)] and β-pyrochlore oxides.[21–25)] In these materials, a guest atom is contained in a cage composed of relatively light atoms and oscillates with a large amplitude in a potential with a strong anharmonicity. Such local oscillation with a large amplitude is called *rattling*, and exotic phenomena induced by rattling have attracted much attention in the research of strongly correlated electron materials with a cage structure.

An example of such active investigations is the study of a magnetically robust heavy-electron behavior observed in $SmOs_4Sb_{12}$.[14)] The electronic specific heat coefficient γ_e is in proportion to the effective mass of electrons, but in this material, γ_e is several hundred times larger than that of a free-electron system and is found to be almost unchanged even if a magnetic field up to 30 T is applied. If the heavy effective mass originates from the quantum criticality due to the traditional Kondo effect with a magnetic origin, γ_e should be significantly suppressed by the applied magnetic field. The origin of the heavy-electron state in $SmOs_4Sb_{12}$ is considered to be electron-rattling interaction. In fact, four- and six-level Kondo systems have been analyzed and the magnetically robust heavy-electron state has been actually obtained.[26–28)] The periodic Anderson–Holstein model has been analyzed using the dynamical mean-field theory, and the mass enhancement due to large lattice fluctuations and phonon softening towards a double-well potential have been addressed.[29–31)]

Kondo phenomena in the conduction electron system coupled with local Jahn–Teller phonons[32,33)] and Holstein phonons[34,35)] have been discussed for the realization of a nonmagnetic Kondo effect. From the numerical evaluation of γ_e in the conduction electron system coupled with local anharmonic Holstein phonons, it has been shown that γ_e is largely enhanced by rattling and is actually robust under an applied magnetic field.[36)] Furthermore, it has been pointed out that the Kondo effect due to rattling should exhibit a peculiar isotope effect, which is experimental evidence of rattling-induced heavy-electron phenomena.[37)] Quite recently, the vibration of magnetic ions has been explicitly included in the spinful Yu–Anderson model, and the two-channel Kondo effect has been comprehensively discussed.[38–40)]

When we turn our attention to the β-pyrochlore oxide KOs_2O_6, significant effects of the rattling of a K ion in a tetrahedral cage composed of O and Os ions have been discussed. The rattling-associated anomaly is found in the form of the first-order structural transition at $T_p \sim 7.5$ K, which is difficult to be influenced by a magnetic field and is

not accompanied by any symmetry breaking.[23,24] It has been reported that electric resistivity is in proportion to T^2 for $T < T_p$, while it behaves as $\propto\sqrt{T}$ for $T > T_p$. In the peculiar behavior at high temperatures, it has been suggested that anharmonic phonons play important roles.[41] The transition at T_p has been discussed in the context of electron-rattling interaction. A possible liquid–gas-type rattling transition and the multipole transition driven by the octupole component of K ion rattling have been pointed out.[42,43] From the analysis of the harmonic Holstein model, it has been reported that the first-order transition from the polaronic state to the bipolaronic state occurs in the strong-interaction region at low temperatures.[44–47]

In this study, to obtain deep insight into the effect of anharmonicity on the polaron–bipolaron transition and the heavy-electron state, we analyze the anharmonic Holstein model using the dynamical mean-field theory (DMFT) in combination with the exact diagonalization method at low temperatures such as 10^{-4} of the conduction electron bandwidth.[48] When the anharmonicity is weak, i.e., for nearly harmonic phonons, we again find the first-order polaron–bipolaron transition due to the observation of a discontinuity in the behavior of physical quantities. When the anharmonicity is increased, the polaron–bipolaron transition temperature is reduced and the critical value of electron–phonon interaction becomes smaller. For a strong anharmonicity, the polaron–bipolaron transition disappears and it becomes to a crossover behavior. We discuss the effect of anharmonicity on the heavy-electron state near the polaron–bipolaron transition and crossover regions.

The organization of this paper is as follows. In §2, we introduce the anharmonic Holstein model and explain the anharmonic potential used in this paper. We also provide a brief explanation of the DMFT. In §3, we discuss the properties of the system obtained using the DMFT. Several physical quantities are discussed when we change the electron–phonon interaction, the anharmonicity of phonons, and temperature. Finally, in §4, we summarize this paper. Throughout this paper, we use such units as $\hbar = k_B = 1$.

2. Model and Method

In this section, we introduce the Hamiltonian as

$$H = \sum_{k\sigma} \varepsilon_k c^\dagger_{k\sigma} c_{k\sigma} + H_{\rm eph}, \tag{1}$$

where ε_k is the energy of conduction electrons, $c^\dagger_{k\sigma}$ is a creation operator for conduction electrons with a wave vector $\boldsymbol{k}$ and a spin σ, and $H_{\rm eph}$ denotes a local electron–phonon term. In the following, we describe $H_{\rm eph}$ and the potential for the vibration of the guest atom. Then, we briefly explain the scheme of the DMFT to solve the Hamiltonian.

2.1 *Electron–phonon coupling term*

We consider a situation in which electrons are coupled with the local oscillation of an atom. Such a situation is expressed by

$$H_{\rm eph} = \sum_i \left[g Q_i (n_i - 1) + \frac{P_i^2}{2M} + V(Q_i) \right], \tag{2}$$

where g denotes the coupling constant between electron density and the oscillation of the atom, i indicates the atomic site, $n_i = \sum_\sigma c^\dagger_{i\sigma} c_{i\sigma}$, $c_{i\sigma}$ is the annihilation operator of an electron with a spin σ at a site i, Q_i is the normal coordinate of breathing-mode oscillation of the atom, P_i indicates the corresponding canonical momentum, M is mass of oscillator atom, and $V(Q_i)$ is a potential for atom, which is expressed by

$$V(Q_i) = k_2 Q_i^2 + k_4 Q_i^4. \tag{3}$$

Here, k_2 and k_4 respectively denote the coefficients for the second- and fourth-order terms of the potential for the atom.

Note that in the coupling between electrons and oscillation, we subtract unity from the electron number for convenience in the numerical calculation. If we do not carry out this subtraction, the electron–phonon coupling is effectively enhanced at doubly occupied sites and it is necessary to prepare a large number of phonon basis to obtain convergent results. Since we are interested in the bipolaronic state, it is crucial to perform the calculation with a significant amount of double occupancy with sufficient precision. Thus, we use the electron–phonon term in eq. (2).

For more calculations, it is convenient to introduce the second-quantized phonon operator by following the standard quantum mechanical procedure. The displacement is expressed by $Q_i = Q_0(b_i + b_i^\dagger)$, where $Q_0 = 1/\sqrt{2M\omega_0}$, ω_0 is the phonon energy, and b_i is the annihilation operator of phonons. Note that Q_0 denotes the amplitude of zero-point oscillation for harmonic phonons. Since we consider the anharmonic oscillation including the case of a negative k_2, we do not impose an explicit relation between k_2 and ω_0.

Then, we rewrite $H_{\rm eph}$ using phonon operators as

$$H_{\rm eph} = \omega_0 \sum_i \Big[\sqrt{\alpha}(b_i + b_i^\dagger)(n_i - 1) + b_i^\dagger b_i + \frac{1}{2} + \beta_2 (b_i + b_i^\dagger)^2 + \beta_4 (b_i + b_i^\dagger)^4 \Big], \tag{4}$$

where α, β_2, and β_4 are given by

$$\alpha = \frac{g^2}{2M\omega_0^3}, \quad \beta_2 = \frac{1}{4}\left(\frac{2k_2}{M\omega_0^2} - 1 \right), \quad \beta_4 = \frac{k_4}{4M^2\omega_0^3}. \tag{5}$$

Among them, α indicates the nondimensional electron–phonon coupling constant, while β_2 and β_4 denote the nondimensional second- and fourth-order anharmonicity parameters, respectively. Note that the anharmonicity of the potential is controlled by adjusting β_2, which becomes both positive and negative, while we always set $\beta_4 > 0$ to restrict the oscillation of an atom in a finite space. We also note that the harmonic case is denoted by $\beta_2 = \beta_4 = 0$.

2.2 *Anharmonic potential*

Now, we discuss the anharmonic potential for the oscillation of an atom. For this purpose, it is convenient to introduce the nondimensional displacement q_i through the relation $q_i = Q_i/Q_0$ in accordance with the second-quantization of a phonon. Using nondimensional displacement, we obtain the potential as

$$V(q_i) = \omega_0 \left[\left(\beta_2 + \frac{1}{4} \right) q_i^2 + \beta_4 q_i^4 \right]. \tag{6}$$

Note that the energy scale of $V(q_i)$ is taken as ω_0.

In Fig. 1(a), we show several anharmonic potentials by changing β_2 for $\beta_4 = 0.02$. For $\beta_2 > -0.25$, the potential

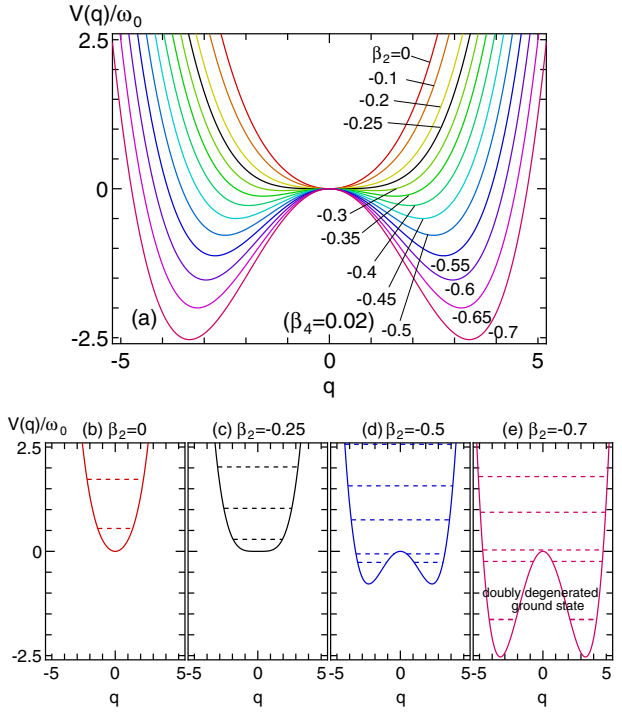

Fig. 1. (Color online) (a) Local phonon potential $V(q)$ for several values of β_2 from 0 to -0.7 with $\beta_4 = 0.02$. (b)–(e) Several typical potentials with $\beta_2 = 0$, -0.25, -0.5, and -0.7, respectively. We show eigenenergy levels with dotted horizontal lines.

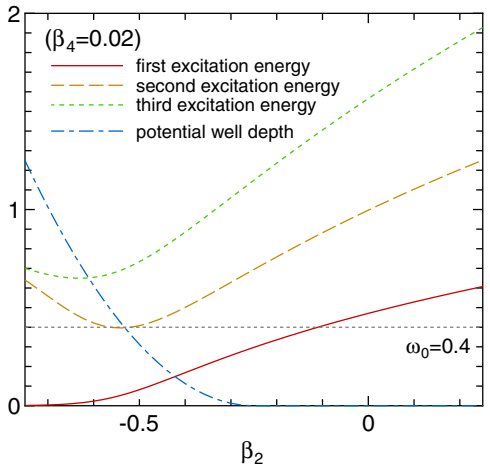

Fig. 2. (Color online) Energies in the local phonon potentials. The first, second, and third excitation energies of the local phonon and the depth of the potential well are shown. The phonon frequency $\omega_0 = 0.4$ is also indicated.

minimum is always situated at $q_i = 0$ and the shape of a single-well potential is similar to that for a harmonic potential. However, in the region of $0 > \beta_2 > -0.25$, the bottom of the potential is found to be wide and flat, since at $\beta_2 = -0.25$, the second-order term of the potential vanishes. When β_2 is decreased from -0.25, the potential shape is changed, since potential minima appear at $\pm q_{\min}$, given by $q_{\min} = \sqrt{(\beta_2 + 1/4)/(2\beta_4)}$. For $\beta_2 < -0.25$, the potential minimum rapidly decrease, leading to the double-well potential. We consider that the decrease in β_2 indicates the increase in anharmonicity.

In Figs. 1(b)–1(e), we show some typical shapes for a single-well type for $\beta_2 = 0$, a flat-bottom type for $\beta_2 = -0.25$, a shallow double-well type for $\beta_2 = -0.5$, and a deep double-well type for $\beta_2 = -0.7$. We also show the eigenenergy levels obtained by the diagonalization of $H_{\rm eph}$. It is observed that the energy levels tend to move to the lower side and that the width between adjacent levels becomes smaller, when β_2 is decreased. In the double-well type cases shown in Figs. 1(d) and 1(e), several levels are found inside the wells. When we further decrease β_2, the levels of the ground and first-excited states exist deep inside the wells and the width between adjacent levels is extremely small. We expect that the ground and first-excited states finally become degenerate for a large negative β_2 with a deep double-well type potential.

In Fig. 2, we show several excitation energies and the depth of the potential well, defined by $V(0) - V(q_{\min})$. We also depict $\omega_0 = 0.4$ line in the graph, which corresponds to the first excitation energy in the harmonic phonon case. When we decrease β_2, i.e., increase anharmonicity, we find that the excitation energies are totally suppressed. For $\beta_2 < -0.25$, the potential wells are formed at $q_i = \pm q_{\min}$. When we decrease β_2, the first excitation energy is gradually decreased and eventually at $\beta_2 \sim -0.7$, it becomes almost zero. On the other hand, the second and third excitation energies are rather increased in the region of $\beta_2 < -0.5$, since the ground-state energy is rapidly decreased.

2.3 *Dynamical mean-field theory*

To solve the model Hamiltonian, it is necessary to use appropriate approximation depending on the problem. Here, we adopt the dynamical mean-field theory (DMFT).[49] In the present case, the model is mapped onto an effective impurity Anderson–Holstein model.[50] In the following, we briefly explain the scheme of the DMFT.

The local electron Green's function $G(\mathrm{i}\omega_n)$ is given by

$$G(\mathrm{i}\omega_n) = \sum_{\boldsymbol{k}} \frac{1}{\mathrm{i}\omega_n - \varepsilon_{\boldsymbol{k}} - \mu - \Sigma(\mathrm{i}\omega_n)}, \tag{7}$$

where ω_n is the fermion Matsubara frequency, given by $\omega_n = \pi T(2n+1)$ with an integer n, T is the temperature, μ is the chemical potential, and $\Sigma(\mathrm{i}\omega_n)$ is the electron self-energy. Note that, in the DMFT, the momentum dependence of the self-energy can be ignored.

To perform momentum summation, it is necessary to specify the lattice type. Here, we consider the Bethe lattice with a semielliptic density of states (DOS) given by

$$\rho(\varepsilon) = \frac{4}{\pi W^2}\sqrt{W^2 - 4\varepsilon^2}, \tag{8}$$

where W is the bandwidth. Using this DOS, we obtain the condition for the local Green's function as

$$G_0(\mathrm{i}\omega_n)^{-1} = \mathrm{i}\omega_n - \mu - \left(\frac{W}{4}\right)^2 G(\mathrm{i}\omega_n), \tag{9}$$

where $G_0(\mathrm{i}\omega_n)$ is the bare local electron Green's function. In the present work, we determine G_0 by the effective impurity Anderson–Holstein model with $\alpha = 0$ in an effective medium determined self-consistently. The effective impurity Anderson–Holstein model with a finite α is solved by the

exact diagonalization method for a finite-sized cluster to obtain $G(i\omega_n)$ at a finite temperature, given by

$$G(i\omega_n) = \frac{1}{Z}\sum_{j,\ell}\frac{e^{-E_\ell/T}+e^{-E_j/T}}{i\omega_n + E_j - E_\ell}|\langle j|c_{i\sigma}|\ell\rangle|^2, \quad (10)$$

where Z is the partition function given by $Z = \sum_j e^{-E_j/T}$, $|j\rangle$ is the eigenstate of the effective impurity Anderson–Holstein model, and E_j is the corresponding eigenenergy.

In the present paper, we use the five-site cluster and the cutoff number N_c for the phonon basis is set to be 12. We have checked the convergence of the calculations in comparison with the results for the six-site cluster and $N_c = 15$. We concentrate our attention to the half-filling case with $\langle n_i\rangle = 1$. We set $W = 4$ and $\omega_0 = 0.4$ in the following calculations. Note that we restrict ourselves to the case with the normal state without any symmetry breaking.

3. Results of DMFT Calculations

3.1 *Lattice fluctuations*

Let us start our discussion about the anharmonicity dependences of various physical quantities for a fixed temperature. First, we discuss the anharmonicity effect on the lattice fluctuation $\sqrt{\langle q^2\rangle}$. In Fig. 3, we show the α dependence of the lattice fluctuation $\sqrt{\langle q^2\rangle}$ for several values of β_2 with $\beta_4 = 0.02$ and $T = 0.0025$. It is found that the curves for $\sqrt{\langle q^2\rangle}$ are monotonically increasing functions. In the following, we discuss the change in the curves for different values of β_2.

When we decrease β_2, i.e., strengthen the anharmonicity, the amplitude of the lattice fluctuations becomes larger. In fact, at $\alpha = 5$, the lattice fluctuation increases from 2.2 to $\sim$4.1 when β_2 decreases from 0 to -0.7. Note that the lattice fluctuation at $\alpha = 0$ already exhibits a similar tendency as it increases from $\sim$0.9 to $\sim$3.2 when β_2 is changed from 0 to -0.7. This tendency can be understood from the potential shape, as shown in Fig. 1. Namely, when β_2 is decreased, the total width of the potential becomes larger and the amplitude of the oscillation in the potential increases owing to thermally activated and quantum tunneling motions.

Next, we comment on the change in the function shape due to β_2. For small absolute values of β_2, the shape of the curve is convex-downward for a small α, while it becomes slightly convex-upward for a large α. For instance, for $\beta_2 = 0$, the change in the behavior can be observed at $\alpha \sim 4$. When the absolute value of β_2 becomes larger, the curve becomes steeper and α at which the convex-downward behavior changes to a slightly convex-upward one becomes smaller. Finally, for $\beta_2 = -0.6$ or -0.7, the behavior for a small α also becomes a linear function. These changes are thought to be caused by the enhancement of the effective electron–phonon interaction coupled with the anharmonic potential.

For a negative β_2 with small absolute value, we find the hysteresis region at approximately α where the increasing behavior is changed. In actual calculations, we obtain two solutions for the same α by gradually increasing and decreasing α. One of the solutions is stable and the other is metastable. Thus, this region can be accounted for by the hysteresis behavior observed in the experimental measurements as well as by the first-order phase transition point where the stable and metastable solutions are switched.

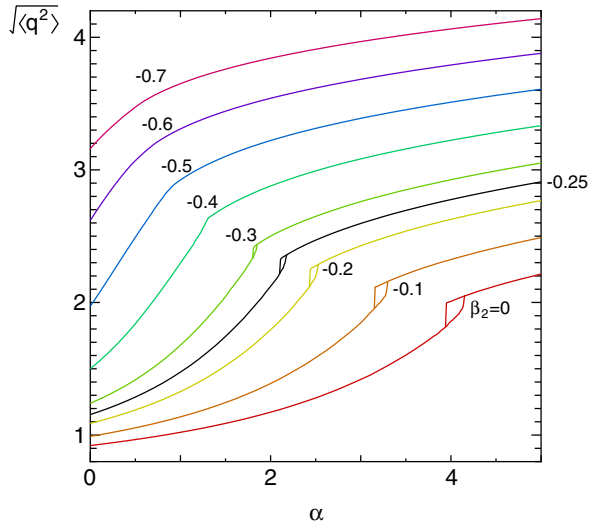

Fig. 3. (Color online) Lattice fluctuations $\sqrt{\langle q^2\rangle}$ vs α for several β_2 values with $\beta_4 = 0.02$ and $T = 0.0025$.

With decreasing β_2, the hysteresis region becomes smaller. For $\beta_2 < -0.5$, it eventually disappears and becomes a smooth crossover between the two solutions. Since the size of the hysteresis region is considered to be related to the energy scale of the first-order phase transition temperature, this result indicates that the anharmonicity suppresses the first-order phase transition. Note that in the present calculations, the systematic reduction in the size of the hysteresis region is obtained at a certain accuracy. When we attempt to quantitatively obtain improved results, it is necessary to resort to an extrapolation technique to estimate the size of the hysteresis region.

3.2 *Double occupancy*

Now we move to the discussion of the electronic states. For this purpose, we examine the behavior of the double occupancy $d = \langle n_\uparrow n_\downarrow\rangle$ as one of the typical physical quantities. In Fig. 4, d is plotted as a function of α for several β_2 values with $\beta_4 = 0.02$ and $T = 0.0025$. For $\alpha = 0$, we find $d = 0.25$, since four local electron states are degenerate in the noninteracting case. When we increase α, d increases monotonically, but the increasing behavior changes during the transition or the crossover. For a small α, d is a convex-downward (almost linear) function at a large (small) β_2, while it is a convex-upward function for a large α. For a sufficiently large α, d asymptotically approaches 0.5, since the vacant and the double-occupied states are degenerate at half-filling in the large α limit.

We remark that d directly indicates the amount of the bipolaronic state in which electrons with antiparallel spins are coupled due to the effective attractive interaction mediated by phonons. Thus, we characterize the two solutions in the hysteresis region using d. Namely, among the two solutions, we define the solution with a larger d as *the bipolaronic solution*, while that with a smaller d is called *the polaronic solution*. Note that, in the definition, the polaronic solution does *not* indicate $d = 0$.

When we consider the β_2 dependence, we again find several remarks that we have already described in the

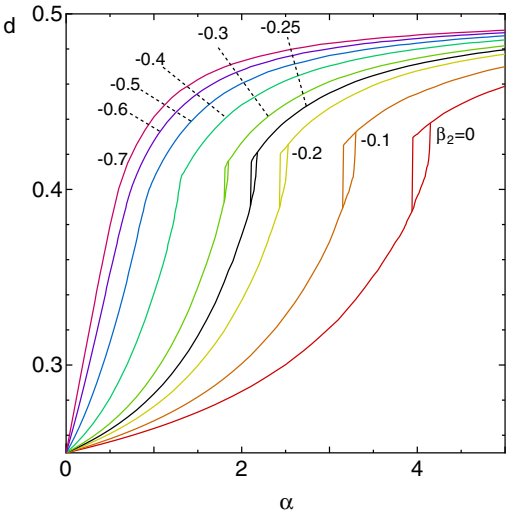

Fig. 4. (Color online) Double occupancy d vs α for several β_2 values with $\beta_4 = 0.02$ and $T = 0.0025$.

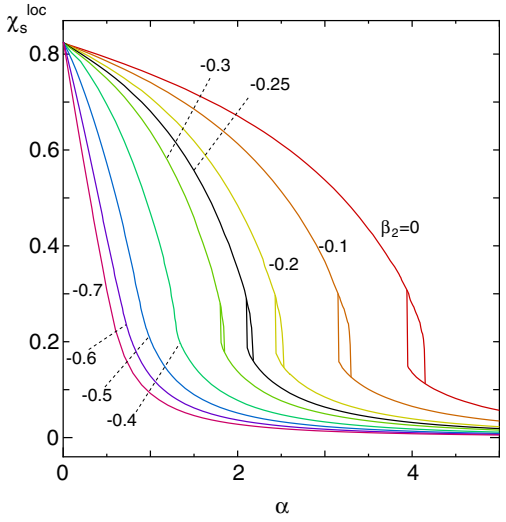

Fig. 5. (Color online) Local spin susceptibility $\chi_s^{\rm loc}$ vs α for several β_2 values with $\beta_4 = 0.02$ and $T = 0.0025$.

previous subsection. Namely, the coexistence region disappears for a small β_2 and the polaron–bipolaron transition or crossover point decreases with decreasing β_2. For a small β_2, a steep increase in d with increasing α is also observed.

3.3 *Local spin and charge susceptibilities*

In the bipolaronic state with a large d, it is expected that the local charge fluctuation is enhanced together with the local lattice fluctuation, while the local moment is suppressed. In fact, from the definition of d in the previous subsection, we obtain $\langle (n_i - \langle n_i \rangle)^2 \rangle = 2d$ and $\langle s_{zi}^2 \rangle = (1 - 2d)/4$, where $s_{zi} = (c_{i\uparrow}^\dagger c_{i\uparrow} - c_{i\downarrow}^\dagger c_{i\downarrow})/2$. Then, we examine the local charge and spin susceptibilities $\chi_c^{\rm loc}$ and $\chi_c^{\rm loc}$, defined as

$$\chi_c^{\rm loc} = \int_0^{1/T} d\tau \langle n_i(\tau) n_i \rangle, \tag{11}$$

and

$$\chi_s^{\rm loc} = \int_0^{1/T} d\tau \langle s_{zi}(\tau) s_{zi} \rangle, \tag{12}$$

respectively.

In Figs. 5 and 6, we show $\chi_s^{\rm loc}$ and $\chi_c^{\rm loc}$, respectively, for several anharmonic potentials with $T = 0.0025$. With increasing α, $\chi_s^{\rm loc}$ is a decreasing function, while $\chi_c^{\rm loc}$ is an increasing function. The degree of decrease or increase tendency is enhanced, when β_2 is decreased, i.e., the anharmonicity is increased. The behavior agrees well with our expectation of the local charge and spin fluctuations, mentioned above. For the solutions with a sufficiently large α, irrespective of β_2, $\chi_s^{\rm loc}$ asymptotically approaches zero, while $\chi_c^{\rm loc}$ approaches a finite specific value, $\sim$400. The behavior has been obtained in the calculations for a harmonic phonon.[47] Thus, the present result confirms that the states with a large α describe the bipolaronic state, in which charge fluctuations are dominant, while spin fluctuations are totally suppressed.

3.4 *Renormalization factor*

In this subsection, we discuss the possibility of the heavy-electron state due to the strong electron–phonon interaction

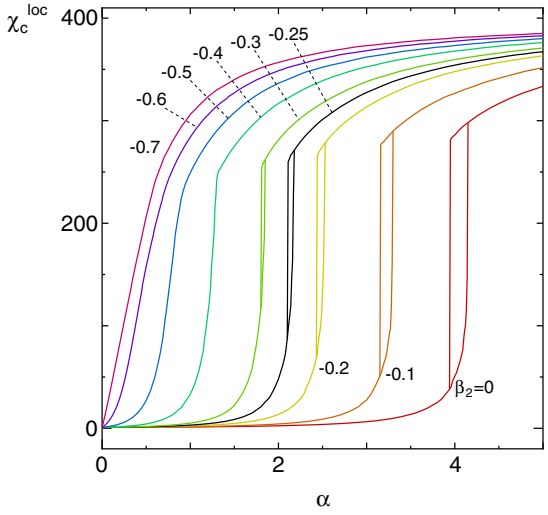

Fig. 6. (Color online) Local charge susceptibility $\chi_c^{\rm loc}$ vs α for several β_2 values with $\beta_4 = 0.02$ and $T = 0.0025$.

with the anharmonicity. For this purpose, we estimate the renormalization factor z defined by

$$z^{-1} = 1 - \left. \frac{d\,{\rm Re}\,\Sigma(\omega)}{d\omega} \right|_{\omega=0}, \tag{13}$$

where $\Sigma(\omega)$ is the electron self-energy with a real frequency ω. In general, z means the renormalization effect of the conduction electron state.

In Fig. 7, we plot z as a function of α for several β_2 values at a low temperature $T = 0.0025$. With increasing α, irrespective of β_2 values, z monotonically decreases and finally goes to zero. As well as other physical quantities discussed in the previous subsections, for a weak-anharmonicity cases with $\beta_2 \geq -0.3$, we find the hysteresis region, in which large- and small-z solutions coexist at the same α. On the other hand, for strong-anharmonicity cases with $\beta_2 < -0.4$, the crossover between the two solutions is observed. The behavior of the decreasing z seems to depend

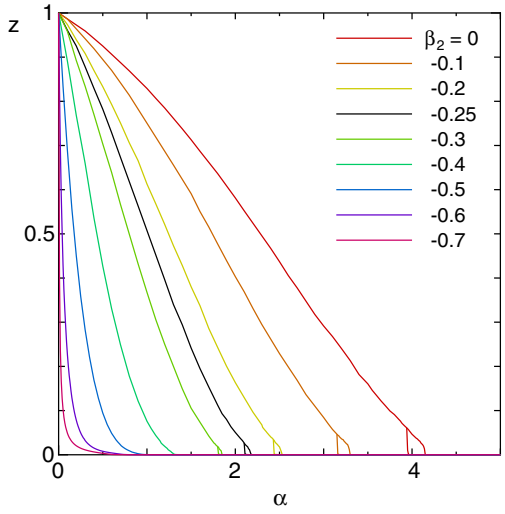

Fig. 7. (Color online) Renormalization factor z vs α for several β_2 values with $\beta_4 = 0.02$ and $T = 0.0025$.

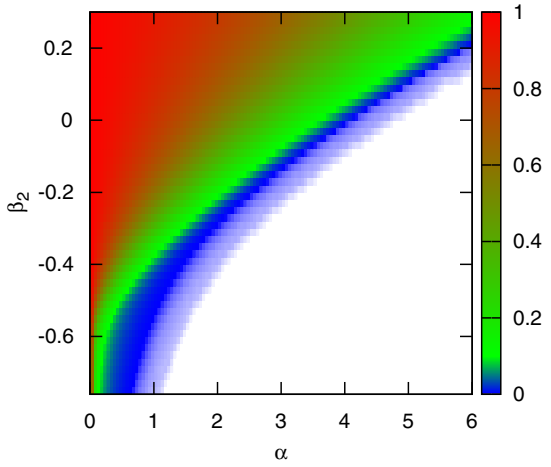

Fig. 8. (Color online) Renormalization factor z on α-β_2 plane for $T = 0.0025$. Depending on the magnitude of z, the phase is shown by color gradation (contrasting density in the case of black-and-white printing): From the left-hand side to the right-hand side of the graph, red (dark gray) for $0.1 \lesssim z \leq 1$, green (light gray) for z on the order of 0.1, blue (black) for $0.001 \lesssim z \lesssim 0.1$, and white for $z < 0.001$ (bipolaronic phase).

on β_2. For the harmonic-like potential with $\beta_2 > -0.25$, z is a slightly convex-upward function for a small α, while for the double-well potential with $\beta_2 < -0.25$, it changes to a convex-downward function. For a smaller β_2, we find a steeper decrease in z for a small α with a polaronic solution.

Here, we recall that the inverse of z indicates the mass enhancement of electrons, expressed by $z^{-1} = m^*/m$, where m^* denotes the effective mass of the conduction electron and m is the bare electron mass. Thus, the small-z solution indicates the formation of a heavy-electron state. Note that the solution in the limit of $z \to 0$ indicates the bipolaronic state with a large α. The heavy-electron state should appear in the polaronic phase in the vicinity of the bipolaronic phase. In this sense, the case in which the solutions with a small z are widely distributed in the parameter region seems to be advantageous for the emergence of the heavy-electron state.

For weak-anharmonicity cases such as $\beta_2 = 0$, small-z solutions with a possible heavy-electron state are found only in the vicinity of the two-solution coexistence region. Thus, there are small possibilities of the heavy-electron state for weak-anharmonicity cases. On the other hand, for strong-anharmonicity case with crossover solutions such as $\beta_2 = -0.5$, z exhibits a convex-downward behavior in the crossover region. Namely, small-z solutions are distributed in the relatively wide region of α. When β_2 is decreased, the tail-like structure can be found in the z behavior in the crossover region, indicating that the region of small-z solutions becomes wide. Therefore, the heavy-electron state due to the electron–phonon interaction is brought about by the large anharmonicity.

To discuss the heavy-electron state in more detail, we show the phase diagram concerning z in the (α, β_2) phase for $T = 0.0025$ in Fig. 8. Here, we define that the heavy-electron state is characterized by the solution with $10 \leq z^{-1} \leq 1000$ and that the corresponding region is indicated in blue (or black, in the case of black-and-white printing). Note that the polaronic metallic region with a large z is expressed in red (dark gray), while the polaronic phase with smaller z is shown in green (light gray). The red (dark gray) and green (light gray) regions are continuously connected and the polaronic phase with a very small z is defined by the heavy-electron state. The bipolaronic insulating phase is expressed by the solution with an extremely small z and is shown in white in the figure.

The green (light gray) region with a smaller z is shown on the left-hand side of the graph, while the white region with $z \to 0$ is shown on the right-hand side of the figure. The blue (black) region with the possible heavy-electron state exists between them. Note that the narrow blue (black) region with a small z on the order of $1/1000$ can be found near the bipolaronic state with $\alpha > \alpha_{c2}$ for large a β_2, where α_{c2} is the upper critical value of the polaron–bipolaron transition. The white region cannot be regarded as the heavy-electron state owing to the strong localization in the bipolaronic state.

When the anharmonicity increases with decreasing β_2, the small-z region expands in the wider region of α around the two-solution coexistence or crossover region. When we decrease β_2, the expansion of the small-z region is pronounced for $\beta_2 \lesssim -0.25$, where the potential shape is changed from the flat single-well type to the double-well type. The present results suggest the close relation between the heavy-electron state and the anharmonicity.

3.5 Electron and phonon spectral functions

Now, we discuss the spectral functions of electrons and phonons. For this purpose, we evaluate the DOS obtained from the imaginary part of Green's function. The electron DOS $\rho_{\rm el}(\omega)$ and the phonon DOS $\rho_{\rm ph}(\omega)$ are respectively given by

$$\rho_{\rm el}(\omega) = -\frac{1}{\pi} \mathrm{Im}\, G(\omega + \mathrm{i}\eta), \tag{14}$$

and

$$\rho_{\rm ph}(\omega) = -\frac{1}{\pi} \mathrm{Im}\, D(\omega + \mathrm{i}\eta), \tag{15}$$

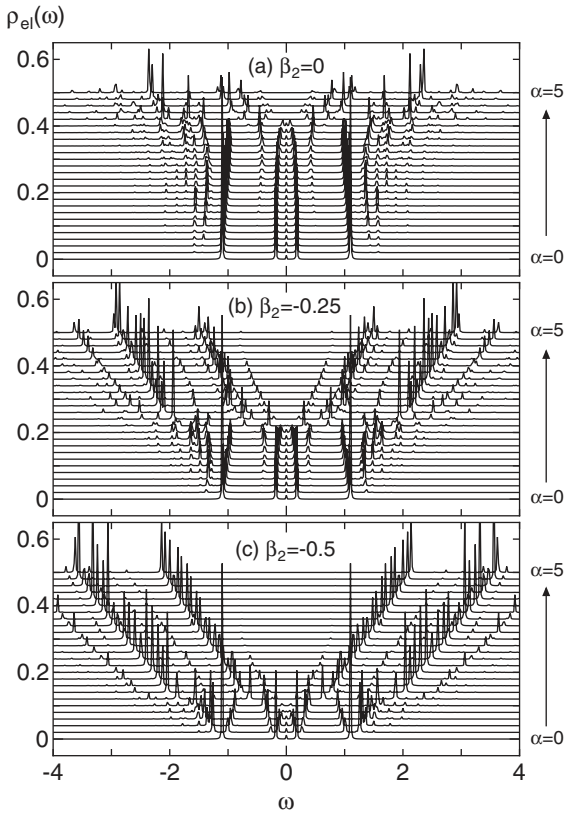

Fig. 9. Electron DOSs $\rho_{el}(\omega)$ for three typical potentials as (a) harmonic type with $\beta_2 = 0$, (b) flat single-well type with $\beta_2 = -0.25$, and (c) double-well type with $\beta_2 = -0.5$. We set $\beta_4 = 0.02$ at $T = 0.0025$. We show the α dependence from 0 to 5 from bottom to top for each panel. For each 0.2 step in the increase in α, the graph is shifted upward by 0.02.

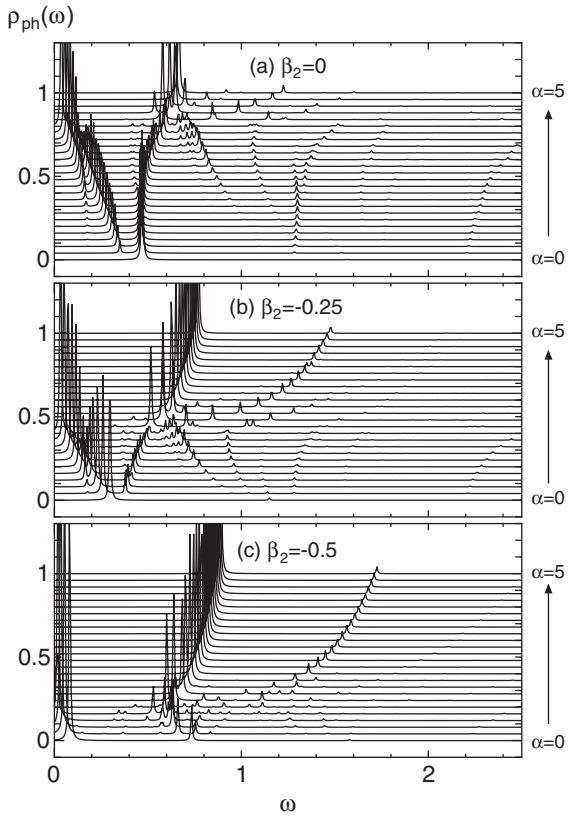

Fig. 10. Phonon DOSs $\rho_{ph}(\omega)$ for three typical potentials as (a) harmonic type with $\beta_2 = 0$, (b) flat single-well type with $\beta_2 = -0.25$, and (c) double-well type with $\beta_2 = -0.5$. We set $\beta_4 = 0.02$ at $T = 0.0025$. We show the α dependence from 0 to 5 from bottom to top for each panel. For each 0.2 step increase in α, the graph is shifted upward by 0.04.

where η is a positive infinitesimal quantity, G is defined in eq. (10), and the phonon Green's function D is given by

$$D(\mathrm{i}\nu_n) = \frac{1}{Z}\sum_{j,\ell}\frac{\mathrm{e}^{-E_\ell/T} - \mathrm{e}^{-E_j/T}}{\mathrm{i}\nu_n + E_j - E_\ell}|\langle j|(b_i + b_i^\dagger)|\ell\rangle|^2. \quad (16)$$

Here, $\nu_n = 2\pi T n$ is the boson Matsubara frequency. Note that we set $\eta = 0.004$ in order to draw the continuous spectrum function for clear visibility.

In Fig. 9, we show the curves for the electron DOS at $T = 0.0025$ for three typical potentials (a) $\beta_2 = 0$, (b) -0.25, and (c) -0.5, corresponding to the harmonic, the flat single-well, and the double-well types, as shown in Figs. 1(b)–1(d), respectively. For each panel, we show the curves in the order of α from bottom to top. Note that, in the two-solution coexistence region, we plot the results for the polaronic metallic solution with a large z.

At $\alpha = 0$, a set of two large peaks for high energy $\omega > 0$ (low energy $\omega < 0$) and a small peak at $\omega = 0$ can be commonly seen in the three panels. Note that the bilaterally symmetric graph is due to the particle–hole symmetry. For a small α, the structure is almost unchanged. On the other hand, for a large α, the set of two large peaks in $\omega > 0$ ($\omega < 0$) moves to the right-hand side (left-hand side) of the graph with increasing α. Then, the disappearance of the peak at $\omega = 0$ is also observed, indicating the disappearance of quasi-particle band. The critical values of the disappearance of the peaks at $\omega = 0$ are $\alpha \sim 4$, 2, and 1 for $\beta_2 = 0$, -0.25, and -0.5, respectively, which agree well with the α which the transition or crossover is indicated.

Note here that the renormalization factor z discussed above should correspond to the decrease in the bandwidth, which is well known as the polaronic band narrowing effect. However, it is difficult to observe such a band narrowing effect for a small α in these graphs, in spite of the significant change in z. This is seemingly incomprehensible at a glance, but similar results have already been found in the harmonic Holstein model.[51–53] According to previous studies, in the polaronic phase, with increasing effect of electron–phonon interaction, the central peak at $\omega = 0$ becomes narrower and more pronounced with the corresponding weight z, while the other peaks with total weights of $1 - z$ exhibit almost no changes. The reason why the other peaks do not move at all is that the Holstein model has few energy distribution corresponding to the upper and lower Hubbard bands, which are split upward and downward depending on the Coulomb interaction. Thus, the conservation of the DOS for a small α is valid, at least within the present calculation on the basis of the exact diagonalization. As for the reproduction of the central peak behavior, it is necessary to improve the precision of the calculation, for instance, by increasing the cluster size.

Next we move to the phonon spectral function. In Fig. 10, we show $\rho_{ph}(\omega)$ at $T = 0.0025$ for three typical potentials with $\beta_2 = 0$, -0.25, and -0.5. At $\alpha = 0$, for each three

panel, distinct peaks can be seen at $\omega \sim 0.43$, 0.3, and 0.04 for $\beta_2 = 0$, -0.25, and -0.5, respectively. These ω values correspond to quasi-harmonic phonons, which agree well with the first excitation energies observed in Fig. 2.

With decreasing β_2, the shift of the peaks to the lower-energy side is indicated. In the polaronic state for small α, the shifts of the low-energy peaks are significant with increasing α, implying the softening of phonons and the divergence of charge susceptibility. The heavy-electron tendency caused by phonon softening due to anharmonicity has been discussed in refs. 54 and 55. In the polaron–bipolaron transition or crossover region, the disappearance of the peaks at lower energy can be seen, suggesting the marked change in phonon properties. The critical value of α at which the lowest energy peak disappears is in good agreement with the transition point or crossover region. In the bipolaronic state, the second lower peaks are continuously connected to those in the polaronic state and they move to the high-energy side with increasing α as well as in the electron spectrum cases.

3.6 *Temperature dependence of physical quantities*

Thus far, we have discussed several physical quantities focusing our attention on the fixed temperature with $T = 0.0025$. In this subsection, we mention the temperature dependence briefly. Here, we consider three typical potentials with $\beta_2 = 0$, -0.25, and -0.5 for $\beta_4 = 0.02$. In Fig. 11, we show the α dependences of several physical quantities such as (a) lattice fluctuation $\sqrt{\langle q^2 \rangle}$, (b) the renormalization factor z, (c) the double occupancy d, (d) the local spin susceptibility $\chi_s^{\rm loc}$, and (e) the local charge susceptibility $\chi_c^{\rm loc}$ for several temperatures from $T = 0.0015$–0.0105.

The marked changes in the physical quantities due to the difference in temperature can be seen only in the vicinity of the two-solution coexistence or crossover region, and the amplitude of the local charge susceptibility. With increasing temperature, the reduction in the size of the two-solution coexistence region is indicated. The edge point for a larger α of the two-solution coexistence region α_{c2} moves to the left-hand side of the graph. As for the shift in α_{c1}, the edge point for a smaller α, it is relatively small compared with that in α_{c2}. Furthermore, α_{c1} and α_{c2} coincide with each other at high temperatures. Then, the two-solution coexistence region disappears and the first-order transition changes to a crossover. Meanwhile, $\chi_c^{\rm loc}$ in the bipolaronic solution for a large α rapidly decreases with increasing T. The temperature dependence of $\chi_c^{\rm loc}$ in the bipolaronic state exhibits the Curie-law behavior $\chi_c^{\rm loc} \propto 1/T$,[47] which is similar to that in the case with the localized spin in the Mott insulator, where the local spin susceptibility shows the Curie law behavior $\chi_s^{\rm loc} \propto 1/T$. In the harmonic case, the $\chi_c^{\rm loc}$ in the present anharmonic case also follows the Curie law.

In the strong-anharmonicity case with $\beta_2 = -0.5$, we point out that the crossover behavior is shown at all temperatures, even below $T = 0.0015$ (not shown here). As indicated in the lowest-energy phonon spectrum in Fig. 10 and the energy levels shown in the bare local phonon potential in Fig. 1(d), the low-temperature crossover is attributed to the small excitation energy of phonons. Namely, the amplitude of the excitation energy is considered

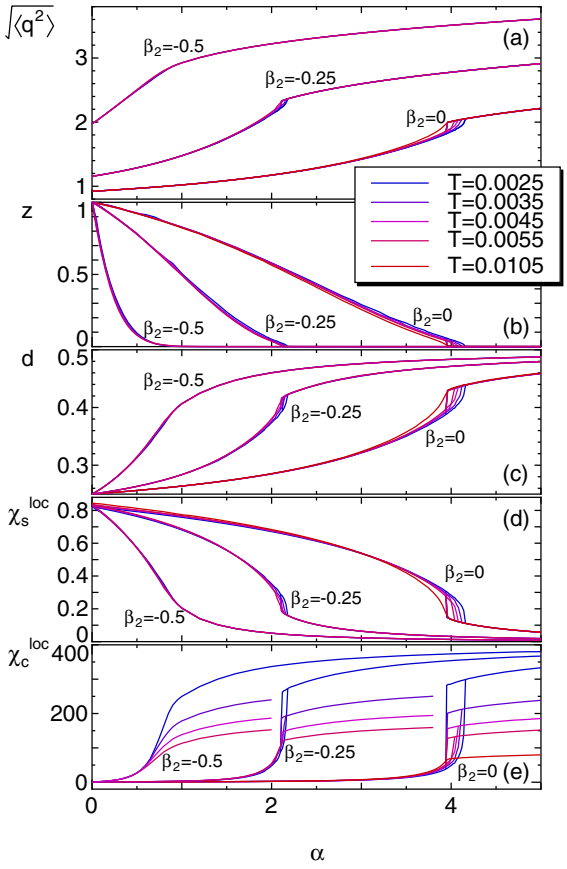

Fig. 11. (Color online) (a) Lattice fluctuation $\sqrt{\langle q^2 \rangle}$ vs α, (b) renormalization factor z vs α, (c) double occupancy d vs α, (d) local spin susceptibility $\chi_s^{\rm loc}$ vs α, and (e) local charge susceptibility $\chi_c^{\rm loc}$ vs α for $\beta_2 = 0$, -0.25, -0.5 with $T = 0.0025$, 0.0035, 0.0045, and 0.0055 with $\beta_4 = 0.02$. In the $\beta_2 = 0$ case, the graph with the crossover result at $T = 0.0105$ is also indicated. Several $\chi_c^{\rm loc}$ dependences for a large α are omitted to avoid overlaps of the graph. Note that $\chi_c^{\rm loc}$ approaches to a finite specific value depending on T for a large α.

to correspond to the energy scale of the polaron–bipolaron transition. Near the crossover region at high temperatures, a smooth tail-like behavior with a small z is observed. For instance, in the graph for $\beta_2 = -0.25$, the tail-like behavior is observed near $\alpha \sim 2.1$ for $T > 0.0055$ around the crossover region. Moreover, for $\beta_2 = -0.5$, such behavior can be found at all the temperature, indicating the possibility of the heavy-electron state.

3.7 *First-order polaron–bipolaron transition*

In the previous subsection, the two-solution coexistence regions are indicated for $\beta_2 = 0$ and -0.25 at low temperatures. Namely, the first-order polaron–bipolaron transition occurs in the region of $\alpha_{c1} < \alpha < \alpha_{c2}$. To discuss this transition, we show the α–T phase diagrams for $\beta_2 = 0$ and -0.25 in Figs. 12(a) and 12(b), respectively, in which we plot α_{c1} and α_{c2} for several T obtained from the discontinuity in the lattice fluctuation.

With increasing T, both α_{c1} and α_{c2} show a decreasing tendency, with the change in the former being moderate, while that in the latter being pronounced. We find that α_{c1} and α_{c2} coincide with each other at a critical point, denoted by α_{cr} or T_{cr}. Above this critical temperature, a smooth crossover is observed instead of a discontinuous change between the polaronic and bipolaronic solutions.

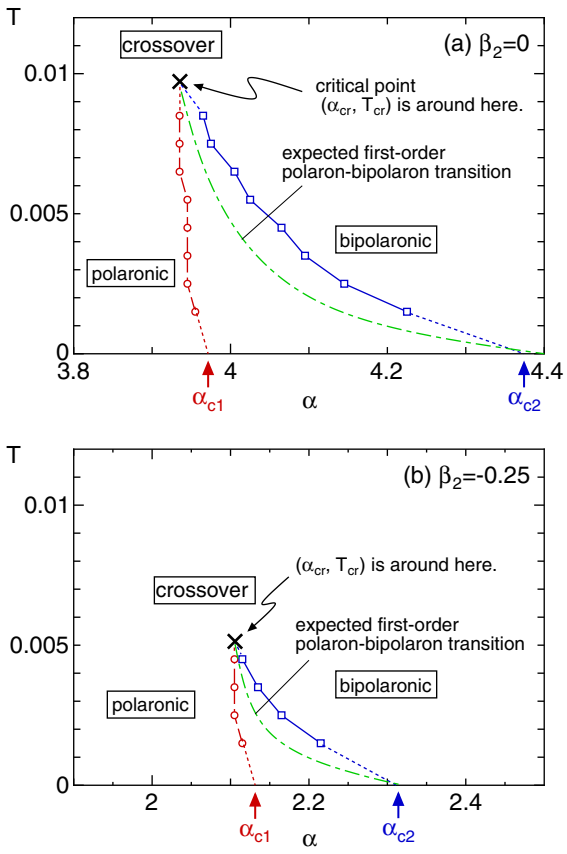

Fig. 12. (Color online) Phase diagrams on α–T plane for (a) $\beta_2 = 0$ and (b) $\beta_2 = -0.25$ with $\beta_4 = 0.02$. In the region $\alpha_{c1} < \alpha < \alpha_{c2}$, both the polaronic and bipolaronic solutions coexist. The dotted-dashed curve shows a possible first-order transition temperature and the cross indicates its critical point. At lower temperatures, we also plot the expected values of α_{c1} and α_{c2} with a dotted line.

For $\beta_2 = 0$ and -0.25, the estimated values of T_{cr} are $\sim$0.01 and $\sim$0.005, respectively. Below T_{cr}, the first-order polaron–bipolaron transition is expected to take place similarly to that in the case with the Mott transition.[49] Then, we plot a possible first-order transition point in the graph. Here, we focus on the largeness of the two-solution coexistence region, i.e., the region width of $|\alpha_{c2} - \alpha_{c1}|$ and the critical temperature T_{cr} height on the α–T plane. It is found that the area for $\beta_2 = -0.25$ is smaller than that for $\beta_2 = 0$ in both the α width and the T_{cr} height. Since the reduction in the area can be associated with the energy scale of the first-order transition, this result suggests that the enhancement of the anharmonicity suppresses the first-order polaron–bipolaron transition.

Then, we discuss the development of the critical point of the first-order polaron–bipolaron transition. In Fig. 13, we show the β_2 dependences of the critical point α_{cr}, T_{cr}. Note here that α_{cr} in the crossover region is determined from the value at which the curvature of the lattice fluctuation $\sqrt{\langle q^2 \rangle}$ changes. In the graph, when β_2 decreases, both α_{cr} and T_{cr} decrease. The decrease in α_{cr} indicates the enhancement of the effective electron–phonon interaction coupled to the anharmonicity. As for T_{cr}, we observe a gradual decrease for a large β_2, while the shape changes to a slightly steeper curve for $\beta_2 \sim -0.25$ and finally approaches zero. This T_{cr} behavior seems to be similar to the β_2 dependence of the first

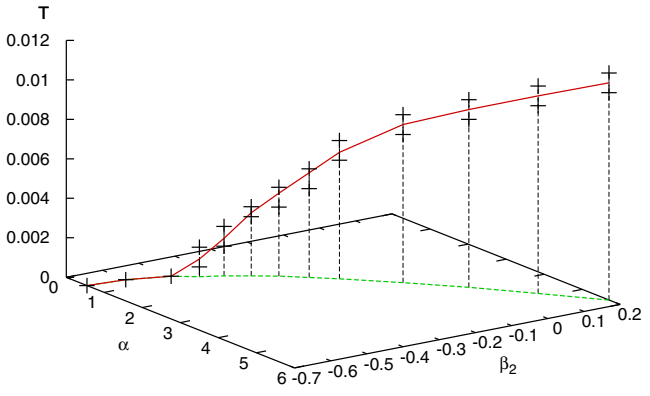

Fig. 13. (Color online) First-order polaron–bipolaron transition critical point α_{cr}, T_{cr} vs β_2 for $\beta_4 = 0.02$. The crosses indicate the temperatures where the crossover solution appears on the higher-temperature side and the coexistence solutions are found on the lower temperature side. The critical points exist on the bars marked by crosses. The expected critical points and the projection onto the $T = 0$ plane are shown as solid and dashed curves, respectively.

excitation energy of phonons in Fig. 2. Thus, the suppression effect is thought to be caused by the reduction in the excitation energy of phonons. For $\beta_2 < -0.5$, we find no evidence of the two-solution coexistence region for the temperature region where we have performed our calculations. For this reason, we set T_{cr} to 0 in Fig. 13; however, we do not exclude the possibility of a polaron–bipolaron transition point with an extremely low transition temperature in the region of $\beta_2 \lesssim -0.5$, since a small but finite excitation energy is indicated in the local phonon problem.

4. Discussion and Summary

In this paper, to discuss the effect of the anharmonicity of phonons on the emergence of the heavy-electron state and the polaron–bipolaron transition, we have analyzed the anharmonic Holstein model, which describes the interaction between conduction electrons and the atom oscillation in the potential with second- and fourth-order anharmonic terms, using the dynamical mean-field theory by the exact diagonalization method. We have obtained various physical quantities as functions of the electron–phonon interaction α for several types of anharmonic potential.

First, we have discussed the effect of anharmonicity on the first-order polaron–bipolaron transition. For a weak-anharmonicity case with a large β_2, with increasing α, we have observed an increase in lattice fluctuation, double occupancy, and local charge susceptibility, but a decrease in the renormalization factor z and local spin susceptibility. Moreover, at low temperatures, evidence of the phase transition from the polaronic state to the bipolaronic state, accompanied by the changes in the physical quantities, is found for a strong-coupling region as the two-solution coexistence region. When temperature increases, the region becomes narrower and it finally disappears at a certain critical temperature, resulting in a smooth crossover between the two states.

The polaron–bipolaron transition behavior has been reported in a previous study with harmonic phonons[47] and there is no qualitative difference between their tendencies. In a previous study with a phonon frequency $\omega_0/W = 0.1$, the

transition temperature is estimated to be on the order of 1/1000 of the bandwidth W. Since the transition is dominated by charge fluctuations and it is a relatively spin-independent phenomenon, we suggest its similarity to the first-order phase transition $T_p = 7.5\,\mathrm{K}$ in the β-pyrochlore oxide KOs_2O_6. Here, we note that in this case, the polaronic (bipolaronic) state corresponds to the $T < T_p$ ($T > T_p$) side. On the other hand, when anharmonicity increases with decreasing β_2, we have indicated several changes such as the increase in the amplitude of the lattice fluctuation, the decrease in the critical value of α, and the transition temperature suppression. Thus, in the anharmonic phonon system, a strong electron–phonon interaction is *not* required for the occurrence of the polaron–bipolaron transition, even though a lower-temperature environment is necessary. This is considered to be advantageous for the explanation of the T_p transition.

Then, let us discuss how the anharmonicity contributes to the heavy-electron state. In this study, we have discussed the effective mass of electrons through the renormalization factor z as functions of α and β_2. With increasing α, z monotonically decreases, namely, the effective mass increases. The heavy-electron state with a small-z solution has been found in the narrow region of the polaronic phase near the polaron–bipolaron transition. Although smaller values of z have been indicated in the bipolaronic solutions, quasiparticles have been destroyed owing to the strong localization tendency. We have found that the possibility of the heavy-electron formation is large in the region in which the small-z solutions are widely distributed. In this sense, the heavy-electron state can be found in the region where the crossover is indicated. The crossover behavior can be seen even in the weak-anharmonicity cases with a large β_2 at high temperatures, although at low temperatures, it becomes a polaron–bipolaron transition with a narrow small-z region in the polaronic phase. Thus, the crossover region with a high possibility of exhibiting the heavy-electron state is only found in the strong-anharmonicity case with small β_2.

Throughout this paper, we have restricted ourselves to the case with the normal state and have not considered the possible phase transition to the charge-density-wave (CDW) state, which is realized in the Holstein model. Within the DMFT, the transition temperature T_{CDW} to the CDW state in the Holstein model was found to be $O(1/100)$ of the bandwidth.[56] As the critical temperature T_{cr} of the polaron–bipolaron transition obtained in the present study is $O(1/1000)$ of the bandwidth and is much smaller than T_{CDW}, it seems to be impossible to observe the polaron–bipolaron transition in the normal state above T_{CDW}. The effect of the frustration, however, is expected to largely suppress T_{CDW}, while keeping T_{cr} almost constant as the polaron–bipolaron transition is exclusively determined by the local DOS, resulting in $T_{CDW} < T_{cr}$. The effect of the anharmonicity β_4 was also found to suppress T_{CDW} except in a small β_4 regime.[57] In addition, in the presence of the Coulomb interaction between electrons, the polaron–bipolaron transition in the Hubbard–Holstein model was found to be realized for a large-g regime, where T_{cr} markedly increases owing to the Coulomb interaction and becomes $O(1/100)$ of the bandwidth,[58] while T_{CDW} is not markedly increases but rather reduced.[59] Therefore, we may expect that the polaron–bipolaron transition will be observed in the normal state above T_{CDW} in the case with the frustration and/or Coulomb interaction. Explicit calculation including the effects of the frustration and the Coulomb interaction together with the effect of the doping[60,61] will be an important future problem to address.

In summary, we have investigated the half-filled anharmonic Holstein model using the dynamical mean-field theory in combination with the exact diagonalization method. We have found that, for the weak-anharmonicity case, the first-order polaronic–bipolaronic phase transition takes place at a critical value of the electron–phonon coupling α, at which each physical quantity shows discontinuity. When the anharmonicity is enhanced, the polaron–bipolaron transition temperature is reduced and the critical value of α decreases. For a strong-anharmonicity case, the polaron–bipolaron transition eventually changes to a crossover, in which a heavy-electron state with a large effective mass is realized owing to the effect of anharmonic phonons.

Acknowledgment

This work has been supported by a Grant-in-Aid for Scientific Research on Innovative Areas “Heavy Electrons” (Nos. 20102008 and 23102709) for the Ministry of Education, Culture, Sports, Science and Technology, Japan. This work has also been supported by a Grant-in-Aid for Specially Promoted Research (No. 18002008) and for Scientific Research (C) (No. 23540443) in part.

1) See, for instance, *Proc. Int. Conf. Heavy Electrons (ICHE2010)*, J. Phys. Soc. Jpn. **80** (2011) Suppl. A.
2) Kondo effect and its related phenomena have been reviewed in J. Phys. Soc. Jpn. **74** (2005) 1–238.
3) J. Kondo: Physica B+C **84** (1976) 40.
4) J. Kondo: Physica B+C **84** (1976) 207.
5) K. Vladár and A. Zawadowski: Phys. Rev. B **28** (1983) 1564.
6) K. Vladár and A. Zawadowski: Phys. Rev. B **28** (1983) 1582.
7) K. Vladár and A. Zawadowski: Phys. Rev. B **28** (1983) 1596.
8) C. C. Yu and P. W. Anderson: Phys. Rev. B **29** (1984) 6165.
9) T. Matsuura and K. Miyake: J. Phys. Soc. Jpn. **55** (1986) 29.
10) T. Matsuura and K. Miyake: J. Phys. Soc. Jpn. **55** (1986) 610.
11) As for a review of filled skutterudites, see H. Sato, H. Suawara, Y. Aoki, and H. Harima: in *Handbook of Magnetic Materials*, ed. K. H. J. Buschow (Elsevier, Amsterdam, 2009) Vol. 18, p. 1–110.
12) T. Goto, Y. Nemoto, K. Sakai, T. Yamaguchi, M. Akatsu, T. Yanagisawa, H. Hazama, K. Onuki, H. Sugawara, and H. Sato: Phys. Rev. B **69** (2004) 180511(R).
13) H. Kotegawa, H. Hidaka, T. C. Kobayashi, D. Kikuchi, H. Sugawara, and H. Sato: Phys. Rev. Lett. **99** (2007) 156408.
14) S. Sanada, Y. Aoki, H. Aoki, A. Tsuchiya, D. Kikuchi, H. Sugawara, and H. Sato: J. Phys. Soc. Jpn. **74** (2005) 246.
15) B. C. Sales, B. C. Chakoumakos, R. Jin, J. R. Thompson, and D. Mandrus: Phys. Rev. B **63** (2001) 245113.
16) T. Goto, Y. Neoto, T. Yamaguchi, T. Yanagisawa, T. Ueno, T. Watanabe, N. Takeda, O. Suzuki, H. Kitazawa, H. Sugawara, and H. Sato: Physica B **383** (2006) 115.
17) M. A. Avila, K. Suekuni, K. Umeo, H. Fukuoka, S. Yamanaka, and T. Takabatake: Phys. Rev. B **74** (2006) 125109.
18) M. A. Avila, K. Suekuni, K. Umeo, H. Fukuoka, S. Yamanaka, and T. Takabatake: Appl. Phys. Lett. **92** (2008) 041901.
19) Y. Nemoto, T. Yamaguchi, T. Horino, M. Akatsu, T. Yanagisawa, T. Goto, O. Suzuki, and A. Dönni: Phys. Rev. B **68** (2003) 184109.
20) Y. Nemoto, T. Yanagisawa, Y. Yasumoto, H. Kobayashi, A.

Yamaguchi, S. Tsuduku, T. Goto, N. Takeda, A. Ochiai, H. Sugawara, H. Sato, and H. Kitazawa: *Proc. Int. Conf. New Quantum Phenomena in Skutterudite and Related Systems (Skutterudite 2007)*, J. Phys. Soc. Jpn. **77** (2008) Suppl. A, p. 153.
21) S. Yonezawa, S. Muraoka, Y. Matsushita, and Z. Hiroi: J. Phys. Soc. Jpn. **73** (2004) 819.
22) S. Yonezawa, S. Muraoka, and Z. Hiroi: J. Phys. Soc. Jpn. **73** (2004) 1655.
23) Z. Hiroi, S. Yonezawa, Y. Nagao, and J. Yamaura: Phys. Rev. B **76** (2007) 014523.
24) Y. Nagao, J. Yamaura, H. Ogusu, Y. Okamoto, and Z. Hiroi: J. Phys. Soc. Jpn. **78** (2009) 064702.
25) K. Umeo, H. Kubo, J. Yamaura, Z. Hiroi, and T. Takabatake: J. Phys. Soc. Jpn. **78** (2009) 123602.
26) S. Yotsuhashi, M. Kojima, H. Kusunose, and K. Miyake: J. Phys. Soc. Jpn. **74** (2005) 49.
27) K. Hattori, Y. Hirayama, and K. Miyake: J. Phys. Soc. Jpn. **74** (2005) 3306.
28) K. Hattori, Y. Hirayama, and K. Miyake: *Proc. 5th Int. Symp. ASR-WYP-2005: Advances in the Physics and Chemistry of Actinide Compounds*, J. Phys. Soc. Jpn. **75** (2006) Suppl., p. 238.
29) K. Mitsumoto and Y. Ōno: Physica C **426–431** (2005) 330.
30) K. Mitsumoto and Y. Ōno: Physica B **403** (2008) 859.
31) K. Mitsumoto and Y. Ōno: J. Phys. Soc. Jpn. **79** (2010) 054707.
32) T. Hotta: Phys. Rev. Lett. **96** (2006) 197201.
33) T. Hotta: J. Phys. Soc. Jpn. **76** (2007) 023705.
34) T. Hotta: J. Phys. Soc. Jpn. **76** (2007) 084702.
35) T. Hotta: Physica B **403** (2008) 1371.
36) T. Hotta: J. Phys. Soc. Jpn. **77** (2008) 103711.
37) T. Hotta: J. Phys. Soc. Jpn. **78** (2009) 073707.
38) S. Yashiki, S. Kirino, and K. Ueda: J. Phys. Soc. Jpn. **79** (2010) 093707.
39) S. Yashiki, S. Kirino, K. Hattori, and K. Ueda: J. Phys. Soc. Jpn. **80** (2011) 064701.
40) S. Yashiki and K. Ueda: J. Phys. Soc. Jpn. **80** (2011) 084717.
41) T. Dahm and K. Ueda: Phys. Rev. Lett. **99** (2007) 187003.
42) K. Hattori and H. Tsunetsugu: J. Phys. Soc. Jpn. **78** (2009) 013603.
43) K. Hattori and H. Tsunetsugu: Phys. Rev. B **81** (2010) 134503.
44) G. Verbist, F. M. Peeters, and J. T. Devreese: Phys. Rev. B **43** (1991) 2712.
45) G. A. Farias, W. B. da Costa, and F. M. Peeters: Phys. Rev. B **54** (1996) 12835.
46) W. B. da Costa and F. M. Peeters: Phys. Rev. B **57** (1998) 10569.
47) T. Fuse and Y. Ōno: J. Phys. Soc. Jpn. **79** (2010) 093702.
48) T. Fuse and Y. Ōno: J. Phys. Soc. Jpn. **80** (2011) SA136.
49) A. Georges, G. Kotliar, W. Krauth, and M. J. Rozenberg: Rev. Mod. Phys. **68** (1996) 13.
50) J. Bauer and A. C. Hewson: Phys. Rev. B **81** (2010) 235113.
51) J. P. Hgue and N. d'Ambrumenil: cond-mat/0106355.
52) D. Meyer, A. C. Hewson, and R. Bulla: Phys. Rev. Lett. **89** (2002) 196401.
53) W. Koller, D. Meyer, A. C. Hewson, and Y. Ōno: Physica B **359** (2005) 795.
54) K. Oshiba and T. Hotta: J. Phys. Soc. Jpn. **80** (2011) SA134.
55) K. Oshiba and T. Hotta: J. Phys. Soc. Jpn. **80** (2011) 094712.
56) J. K. Freericks and M. Jarrell: Phys. Rev. B **50** (1994) 6939.
57) J. K. Freericks, M. Jarrell, and G. D. Mahan: Phys. Rev. Lett. **77** (1996) 4588.
58) T. Fuse and Y. Ōno: Physica C **470** (2010) S701.
59) J. K. Freericks and M. Jarrell: Phys. Rev. Lett. **75** (1995) 2570.
60) M. Capone, G. Sangiovanni, C. Castellani, C. Di Castro, and M. Grilli: Phys. Rev. Lett. **92** (2004) 106401.
61) K. Mitsumoto and Y. Ōno: J. Magn. Magn. Mater. **310** (2007) 419.